Towards Mesh-Free Patient-Specific Mitral Valve Modeling

Judit Ros[1(✉)], Oscar Camara[1], Uxio Hermida[2], Bart Bijnens[1,3], and Hernán G. Morales[2]

[1] Physense, BCN MedTech, Department of Information and Communication Technologies, Universitat Pompeu Fabra, Barcelona, Spain
juditros01@estudiant.upf.edu
[2] Philips Research Paris, Suresnes, France
[3] ICREA, Barcelona, Spain

Abstract. Computational modeling is a tool that has gained importance recently to better understand valve physiopathology, to assess safety and efficacy of cardiovascular devices and as a supporting tool for therapy planning. Mesh-based methods, such as the Finite Element Method (FEM), have shown high accuracy and application modeling the mitral valve (MV). However, when it comes to irregular and complex geometries, FEM techniques suffer from well-documented limitations, such as the labor and time-consuming intrinsic need of a mesh. In this work, novel structural models of the MV and mitral valve regurgitation (MVR) dynamics are presented using a mesh-free method. Obtained results show that the developed models are capable of reproducing MV and MVR behaviour with good agreement with respect to both in-vivo and in-silico studies, in terms of valve closure and opening, valve deformation, as well as stress magnitudes. This paper shows that mesh-free methods have the potential to become a powerful alternative to the currently most used modeling approaches.

Keywords: SPH · Smoothed particles hydrodynamics · Computational modeling · Mitral valve · Mitral valve regurgitation · Mesh-free

1 Introduction

The mitral valve (MV) is a complex cardiac valve located between the left atrium and ventricle. Its structure involves the mitral annulus ring, the anterior and posterior leaflets, both papillary muscles (PM) and some tendinous chords named chordae tendineae that link the leaflets with the PM. In light of this complexity, the development of computational models is a powerful instrument to quantify and further understand valve function both in healthy and diseased conditions. The predictive behaviour of modeling has also the potential to become a strong tool to assist medical decisions, as well as playing an important role in regulatory

E. Puyol Anton et al. (Eds.): STACOM 2020, LNCS 12592, pp. 66–75, 2021.
https://doi.org/10.1007/978-3-030-68107-4_7

pathways, speeding up the incorporation of new cardiovascular devices to the market. To that end, models not only need to be accurate, reliable and robust, but also efficient enough to be used by industry and in a clinical environment.

In the field of cardiac biomechanics, numerical mesh-based approaches, such as the Finite Element Method or Finite Volume Method, have been largely used to solve solid and fluid dynamics problems related to the MV, showing great performance and reliability [1]. Nevertheless, these techniques suffer from well-documented limitations, including the need of high computational cost and time algorithms to handle contact between structures or to represent large deformations [2]. Besides, when coping with irregular geometries such as the MV, mesh generation demands for laborious and manual editing workload, not only being one of the most time-consuming steps of the modeling procedure, but also obstructing the processing of large amount of data.

Contrarily to mesh-based techniques, mesh-free methods, such as Smoothed Particles Hydrodynamics (SPH), may offer some advantages due to the no need of a mesh, such as the calculation of the interaction between implicit surfaces, including solid-solid (contact) and solid-fluid. Also more irregular segmentations can be taken as geometrical input since the neighbour search implicitly smooths those local irregularities. These features are especially interesting for cardiac valve modeling.

Although mesh-free approaches are not as mature as mesh-based ones and have been mostly used to solve fluid dynamics equations, recent developments in SPH have allowed the modeling of a wider range of problems, including cardiac electromechanics [3] and biomechanics [4], being a promising alternative to mesh-based methods. Nevertheless to our knowledge, there is no SPH structural 3D model of the MV nor any of its pathological behaviours. Therefore, the main objectives of this work were: 1) developing a 3D image-based mesh-free structural model of the MV using SPH; and 2) proposing different strategies to model diseased mitral valve regurgitation (MVR) cases.

2 Materials and Methods

2.1 SPH Continuum Mechanics

Total lagrangian SPH discretization was used in order to solve the continuous mechanics equations describing the MV dynamics. The interested reader is referred to [4] for further details. In SPH, the domain is divided in a set of moving particles with no connectivity among them. A function f_i is defined for each particle, which can be approximated by Eq. (1). In this work, the kernel used was the C2-Wendland Kernel, with the kernel correction detailed in [5].

$$f_i = \sum_{j=N_i} f_j V_j W_h(r_{ij}), \tag{1}$$

where the sub-index i is the particle of interest and the j corresponds to a particle inside the neighbourhood of i, denoted as N_i. Let V_j be the volume of the

particle j and $W_h(r_{ij})$ the kernel function, which depends on h, corresponding to the size of the support domain around particle i, and is evaluated in the vector $r_{ij} = x_i - x_j$, with x being the particle position.

To model MV solid mechanics four equations were used. Firstly, the momentum conservation in the reference configuration is expressed as follows:

$$\frac{\partial^2 x_i}{\partial t^2} = \frac{1}{\rho_0} \sum_{j \in N_i} V_j (\mathbf{P}_{ji} - \mathbf{\Pi}_{0ij}) \nabla_0 \tilde{W}_h(r_{ij}) + b_i, \tag{2}$$

where the sub-index 0 denotes the quantity in the reference configuration (at time $t = 0$), ρ is the density, $\mathbf{P}_{ji}$ indicates the difference between the first Piola-Kirchoff stress tensor of particles i and j, and b_i is the sum of external body forces being applied on the particle i, such as gravity, contact (if the particle lays on the surface) or the force exerted by the chordae apparatus, explained in detail in Sect. 2.3. The tensor $\mathbf{\Pi}_{0ij}$ is introduced as an artificial viscosity to compensate local particle oscillations [6]. Secondly, the continuity equation is determined as $\rho_i = \frac{\rho_0}{J_i}$, being J the determinant of the tensor $\mathbf{F}$. Finally, the deformation gradient tensor $\mathbf{F}$ and the neo-Hookean constituve law are given as:

$$\mathbf{F}_i = \frac{\partial x_i}{\partial X_i} = \sum_{j \in N_i} V_j r_{ij} \nabla_0 \tilde{W}_h(r_{ij}), \tag{3}$$

$$\mathbf{P_i} = \mu J_i^{-\frac{2}{3}} (\mathbf{F}_i - \mathbf{F}_i^{-T} (\frac{1}{3} tr(\mathbf{F}_i \cdot \mathbf{F}_i^T))) + \mathbf{F}_i^{-T} (p_i J_i), \tag{4}$$

where the second term on the right is included to reinforce incompresibility with the Lagrange multiplied $p_i = K(J_i - 1)$, being K the bulk modulus.

2.2 Contact with SPH

The frictional contact algorithm based on ideal plastic collision developed by Wang et al. [7] was used. In contrast to most mesh-free contact approaches [8,9], this algorithm avoids particle penetration without the need of a penalization coefficient.

Briefly, contact occurs when a particle i is near a non-neighbour particle k within a given distance δ_c. Once contact is detected, the relative velocity v_{ik} is computed and weighted by their mass ratio $\zeta_m = \frac{m_i}{m_i + m_k}$, being m the particle mass. A contact force $f_{ik,c}$ is then applied from particle k to particle i calculated as follows:

$$f_{ik,c} = \frac{\zeta_m (v_{ik,n} + v_{ik,t})}{\triangle t}, \tag{5}$$

where $v_{ik,n}$ and $v_{ik,t}$ are the normal and tangential relative velocities between particle i and the colliding particle k. The normal component $v_{ik,n}$ is calculated by projecting v_{ik} in the average normal direction $\bar{n}$, determined following the formulation from Seo and Min [10]. Finally, the tangential component $v_{ik,t}$ is computed as follows:

$$v_{ik,t} = \min\{v_{ik} - v_{ik,n},\ \ \mu|v_{ik,n}|\frac{v_{ik} - v_{ik,n}}{|v_{ik} - v_{ik,n}|}\} \tag{6}$$

where μ is the friction coefficient.

2.3 Mitral Valve Simulations

A MV geometry extracted from the segmentation of a Computed Tomography (CT) scan of a patient diagnosed with MVR was used as the starting point for this model. Specifically, the valve used was *case 03 user 01* retrieved from *zenodo.org* [11]. A manual remodeling was performed to the original geometry in order to reduce leaflets stenosis. Two extra particle layers were added to generate a constant total valve thickness of 1 mm. The resulting geometry included 2699 regularly distributed particles and a valve surface area of 4.65 cm^2.

The MV leaflets were modeled as an hyperelastic material following a neo-Hookean law, as presented in Equation (4). Previously reported Young's Modulus for modeling the MV leaflets ranged from 0.8 to 9 MPa [12]. In this work, both leaflets were assumed to have a Young's Modulus of 1.5 MPa. The Poisson's Ratio was set to 0.49 to model leaflets nearly incompressible behaviour [13].

Chordae tendineae were modeled as a set of 156 straight springs linking the PM tips with the leaflets free edges, shown in Fig. 2a. Each spring offers a resistance f_s against the motion towards the atrium, applied only when the spring is stretc.hed and defined with the following equation:

$$f_s = \begin{cases} (L - pL_0)K & if L \geq pL_0 \\ 0 & if L < pL_0 \end{cases} \tag{7}$$

K is the stiffness coefficient and L is the current distance from the corresponding PM to the particle anchored. L_0 is the end-diastolic distance between the PM and the anchored leaflet particle, and p is a percentage pre-multiplying this distance. Parameters K and p were empirically tuned until a complete valve closure was ensured. Since the assumption of linear elasticity of the chords, its distribution and number are unknown; it is not possible to compare the values of these parameters with previous studies.

PM tips were represented as two moving 3D Cartesian coordinates. The motion was described following [14]. Besides, a time-varying relative transvalvular physiological pressure was uniformly applied to particles facing the ventricle, defined accordingly to [15]. Both are shown in Fig. 1 and were assumed to be the same for all models. Finally, mitral annulus ring particles were considered to be fixed.

2.4 Mitral Valve Regurgitation Simulations

Three strategies to model different cases of MVR were proposed. Firstly, primary MVR (PMVR) was modeled. Chordae degeneration is the most prevalent cause

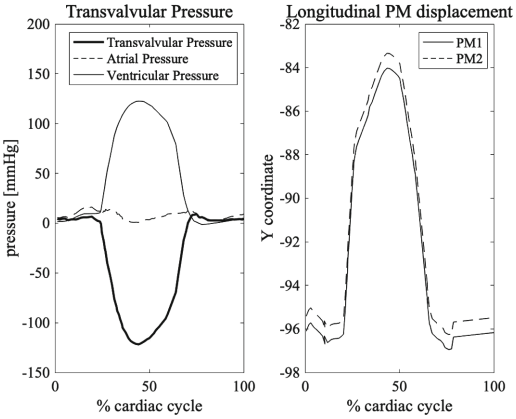

Fig. 1. Physiological transvalvular pressure and PM motion over one cardiac cycle in the longitudinal (Y) direction, corresponding to the ventricular apex to mitral annulus direction.

of PMVR and it is characterized by a decreased stiffness and increased elongation of a specific group of chordae. To mimic this pathological mechanism, the chordae stiffness parameter K from 50 chordae attached to the P1-P2 scallops was decreased 20%. Following Carpentier's classification, P1-P2 scallops corresponded to the anterolateral and middle segments of the posterior MV leaflet. The remaining chordae parameters were the same as in the healthy case.

The second modeled pathological case, named Traumatic MVR (TMVR), corresponded to a more severe case of PMVR posterior to a traumatic injury. A total rupture of the same 50 chords considered in PMVR was simulated, corresponding with a valve with no chordae linked to the P1-P2 scallops.

Finally, the last pathological condition modeled was secondary MVR (SMVR), which is caused by mitral annulus dilatation and PM displacement secondary to a global remodeling of the left ventricle. Therefore, the strategy followed in this case was a dilatation of the valve annulus, together with an apically and laterally translation of the PM. The SMVR annular and PM dimensions can be appreciated in Fig. 2b.

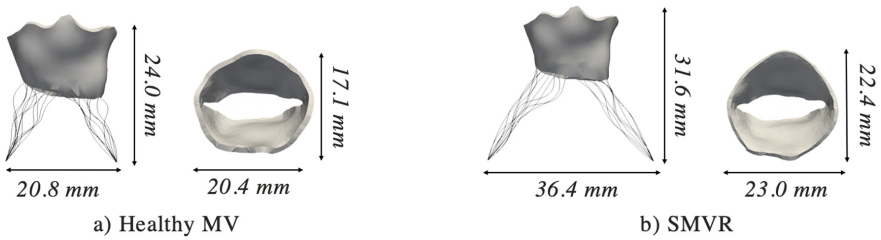

Fig. 2. PM and annulus dimensions in a) healthy and b) SMVR case.

3 Results

The structural healthy MV dynamics in relation to the transvalvular pressure applied during one cardiac cycle are shown in Fig. 3a. The valve remained opened between the 0–20% of the cardiac cycle, corresponding to diastole. Valve closing started at the 25% of the cycle, coinciding with an increase in the ventricular pressure. Valve reopened at the 70% of the cycle, when a decrease in the ventricular pressure is applied.

Under SMVR condition, the valve showed a loss of leaflets coaptation during systole, preventing the valve from closing. The leaflets non-coaptation can be appreciated in Fig. 3b between the 30–60% of the cardiac cycle. It appeared as a consequence of the mitral annulus and PM remodeling.

In the case of PMVR and TMVR, a prolapse into the left atrium was observed during the 45–60% of the cardiac cycle. This prolapse is shown in Fig. 4. The prolapse occurred in the area where the chords were damaged or removed. As expected, in TMVR a more severe prolapse compared to the PMVR was appreciated, due to the chordae rupture.

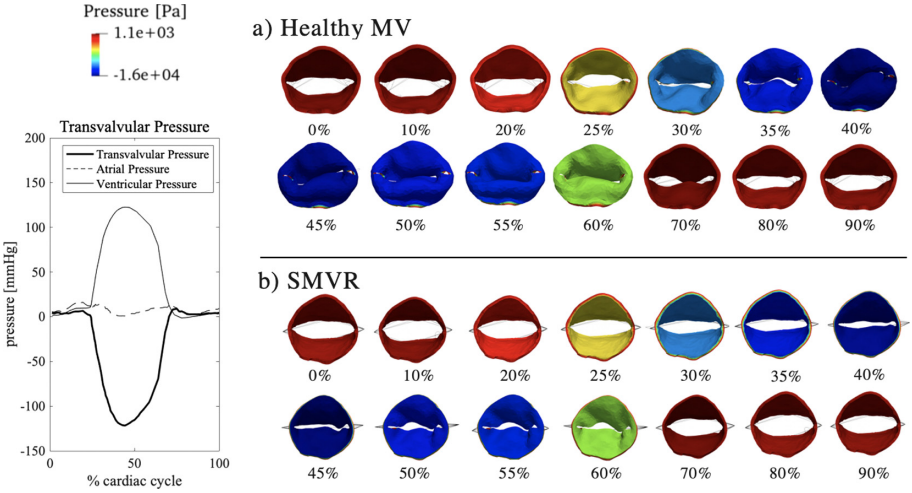

Fig. 3. Valve dynamics over time [%] for healthy and SMVR cases.

In Fig. 5, peak systolic maximum principal stresses are shown. The healthy valve condition presented a mean stress of 127.7 kPa. Higher stresses up to 1 MPa were appreciated in the valve commissures and P1 leaflet scallop, resulting from the non-symmetry of the geometry.

An increase of stresses in the anterior leaflet was clearly visible in the PMVR and TMVR cases, highlighting the peak stresses reached in the annular part of the same leaflet up to 1 MPa. The stress increase was consequence of the larger local deformation that occurred in that area when the prolapse was created. In

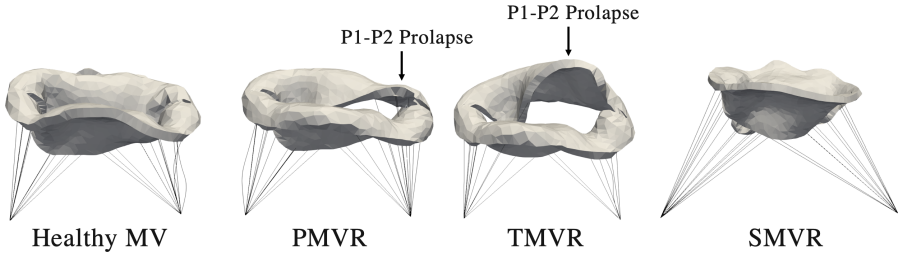

Fig. 4. Anterior view of all cases during systole.

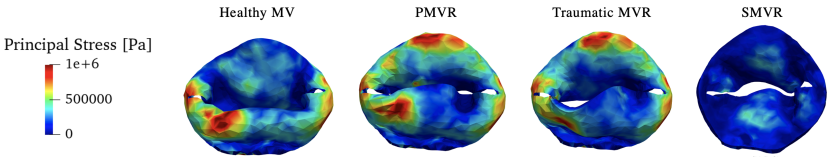

Fig. 5. Maximum peak systolic principal stress.

the healthy case, this relative large deformation did not take place, since the contact with the posterior leaflet prevented it. In the prolapsed P1-P2 scallops, a slight decrease on stresses was appreciated as a result of the lower deformation compared to the healthy case, where the contact with the anterior leaflet prevented tissue free motion. Globally, the overall mean systolic stresses increased up to 145.5 kPa in PMVR and 143.6 kPa in TMVR conditions. The increase in the mean stress is mainly due to the rise in stresses near the annumus. In Fig. 4, the deformation that leads this stresss increment is appreciated.

Stress distribution for the SMVR case greatly differed with the previous states. Here, a generalized reduction on both leaflets stresses was observed, decreasing the mean systolic stress to 68.3 kPa. This significant reduction in the stresses is due to the imposed limited motion of the SMVR state compared to the healthy case.

4 Discussion

The first aim of our work was to develop a 3D image-based mesh-free MV model using SPH. This model was verified with respect to physiological valve dynamics, in term of the overall shape, opening and closure, for given boundary conditions, naming pressure, PM motion and chordae modeling. The contact algorithm properly worked, preventing particle penetration. Moreover, it is coherent with previous mesh-based simulations in terms of stress range. Difference in the stress distribution and values with respect to previous mesh-based simulations are due to the differences in the anatomy, as well as boundary condition.

The second objective was developing some strategies to simulate MVR. The mechanisms responsible for diseased valves were also well modeled as shown with

the PMVR, TMVR and SMVR simuations. In the first two, a damage/rupture of the chords did lead to a prolapse, which is indicative of MVR pathology [16,17]. This prolapse was located in the region where the chords properties were modified. Similarly to [18], the prolapse in the PMVR condition was less severe than in the case of TMVR, since chords were only damaged in the first case and removed in the second one. In the case of SMVR, a dilated heart did influence the performance of the whole valve apparatus even if the valve was healthy. A general leaflets loss of coaptation was observed, commonly presented in SMVR disease [19].

Regarding peak systolic principal stresses, they were found to be between 10–370 KPa in the P2-P3 posterior leaflet scallops and 100–520 KPa in the anterior leaflet of the healthy case, respectively. These ranges agree with previously reported mesh-based analysis [18,20]. For instance, in [20], reported peak systolic stresses ranged from 60 to 270 KPa and 130 to 540 KPa in the posterior and anterior leaflets, respectively. Nevertheless, high stress regions were observed in the valve commissures and P1 scallop of the posterior leaflet, which seems to be consequence of the geometry used.

In PMVR and TMVR cases, an increase on the the anterior leaflet stresses was found. High stress values were observed near the annular region, as in [17]. Besides, a slight decrease on the stresses of the prolapsing scallop was found, also observed, for example, in [18]. SMVR condition showed a 53% decrease of the mean leaflets stresses compared to the healthy case, as a result of the limited deformation of both leaflets due to the annulus dilatation and restricted PM motion.

This work can be complemented with previous efforts where SPH is used to simulate fluid flow in complex cardiac cavities and around valves [21,22], aiming at a pure mesh-free solver for valve dynamics. Although, the use of SPH has been already proposed for FSI problems, including mitral valve opening [23,24], those studies serve as a base since they used 2D idealized geometries, elastic materials and do not consider neither contact mechanics nor PM influence on valve dynamics.

4.1 Limitations

This study is not excluded from limitations. Firstly, this work is a proof of concept for mitral valve modeling using a 3D mesh-free approach and therefore only one image-based geometry was study. A larger set of geometries will be used in the future to test the robustness of the method when changing the geometries. Secondly, only the open valve was available from the patient and therefore, clinical claims cannot be derived from this study. Additional patient data, such as papillary tips, annulus motion and pressure condition are required. Finally, a sensitivity analysis of particle resolution and SPH parameters, including frictional coefficient and kernel size needs to be conducted for complex anatomies.

5 Conclusion

In this work, the first 3D image-based mesh-free structural model of the MV was proposed and developed. Additionally, strategies to reproduce MVR mechanisms were proposed and deeply analyzed. Valve dynamics for healthy and diseased scenarios were qualitative and quantitative evaluated. Results were verified against previous studies with good agreement, in terms of valve closure and opening, as well as deformation and stress ranges. We have demonstrated that SPH-based models have the potential to become an alternative to mesh-based approaches in the modeling of both healthy and diseased MV cases.

Acknowledgments. We gratefully acknowledge clinicians from the Cardiology Service of Hospital Clínic (Barcelona) for clinical consultation.

References

1. Gao, H., et al.: Modelling Mitral Valvular Dynamics - current trend and future directions: review of MV modelling. Int. J. Numer. Meth. Biomed. Eng. **33**(12) (2016)
2. Zhang, L., Ademiloye, A., Liew, K.: Meshfree and particle methods in biomechanics: prospects and challenges. Arch. Comput. Meth. Eng. **26**, 1547–1576 (2019)
3. Lluch, E., et al.: Calibration of a fully coupled electromechanical meshless computational model of the heart with experimental data. Comput. Meth. Appl. Mech. Eng. **364**, 112869 (2020)
4. Lluch, È., De Craene, M., Bijnens, B., Sermesant, M., Noailly, J., Camara, O., Morales, H.G.: Breaking the state of the heart: meshless model for cardiac mechanics. Biomech. Model. Mechanobiol. **18**(6), 1549–1561 (2019). https://doi.org/10.1007/s10237-019-01175-9
5. Chen, J., Beraun, J., Carney, T.: A corrective smoothed particle method for boundary value problems in heat conduction. Int. J. Num. Meth. Eng. **46**(2), 231–252 (1999)
6. Gray, J., Monaghan, J., Swift, R.: SPH elastic dynamics. Comput. Meth. Appl. Mech. Eng. **49**(50), 6641–6662 (2001)
7. Wang, J., Chan, D.: Frictional contact algorithms in SPH for the simulation of soil-structure interaction. Int. J. Num. Anal. Meth. Geomech. **38**(7), 747–770 (2014)
8. Xiao, Y.H., et al.: Simulation of normal perforation of aluminum plates using axisymmetric smoothed particle hydrodynamics with contact algorithm. Int. J. Comput. Meth. **10**(3), 1350039 (2013)
9. Liu, M.B., Liu, G.R.: Smoothed particle hydrodynamics (SPH): an overview and recent developments. Arch. Comput. Meth. Eng. **17**, 25–76 (2010)
10. Seo, S., Min, O.: Axisymmetric SPH simulation of elasto-plastic contact in the low velocity impact. Comput. Phys. Commun. **175**, 583–603 (2006)
11. Tautz, L., et al.: CT segmented mitral valves in open state. Zenodo (2019)
12. Lim, K., Yeo, J., Duran, C.: Three-dimensional asymmetrical modeling of the mitral valve: a finite element study with dynamic boundaries. J. Heart Valve Dis. **14**(3), 386–392 (2005)
13. Maisano, F.: An annular prosthesis for the treatment of functional mitral regurgitation: finite element model analysis of a dog bone-shaped ring prosthesis. Ann. Thorac. Surg. **79**(4), 1268–1275 (2005)

14. Sanfilippo, A., et al.: Papillary muscle traction in mitral valve prolapse: quantification by two-dimensional echocardiography. J. Am. Coll. Cardiol. **19**(3), 1268–1275 (1992)
15. Kaiser, A., McQueen, D., Peskin, C.: Modeling the Mitral Valve. Wiley, New York (2019)
16. Gabriel, V., Kamp, O., Visser, C.: Three-dimensional echocardiography in mitral valve disease. Eur. J. Echocardiogr. **6**(6), 443–454 (2005)
17. Rim, Y., et al.: Personalized computational modeling of mitral valve prolapse: virtual leaflet resection. PLoS ONE **10**(6), e0130906 (2015)
18. Caballero, A., et al.: New insights into mitral heart valve prolapse after chordae rupture through fluid-structure interaction computational modeling. Sci. Rep. **8**, 17306 (2018)
19. Izumi, S., et al.: Mechanism of mitral regurgitation in patients with myocardial infarction: a study using real-time two-dimensional doppler flow imaging and echocardiography. Circulation **76**(4), 777–785 (1987)
20. Votta, E., et al.: Mitral valve finite-element modelling from ultrasound data: a pilot study for a new approach to understand mitral function and clinical scenarios. Philos. Trans. R. Soc. A Math. Phys. Eng. Sci. **366**(1879), 3411–3434 (2008)
21. Yuan, Q., et al.: Fluid structure interaction study of bioprosthetic heart valve with FESPH method. Int. J. Adv. Comput. Technol. **8**, 695–702 (2013)
22. Mao, W., et al.: Fully-coupled fluid-structure interaction simulation of the aortic and mitral valves in a realistic 3D left ventricle model. PLOS ONE **12**(9), e0184729 (2017)
23. Antonci, C., et al.: Numerical simulation of fluid-structure interaction by SPH. N. Engl. J. Med. **339**(24), 1725–1733 (1998)
24. Amanifard, N., Rahbar, B., Hesan, M.: Numerical simulation of the mitral valve opening using smoothed particle hydrodynamics. In: Proceedings of the World Congress on Engineering, vol. 3 (2011)